Involvement of autophagy in the maintenance of rat intervertebral disc homeostasis: an in-vitro and in-vivo RNA interference study of Atg5

Tsujimoto, R. ; Yurube, T. ; Takeoka, Y. ; Kanda, Y. ; Miyazaki, K. ; Ohnishi, H. ; Kakiuchi, Y. ; Miyazaki, S. ; Zhang, Z. ; Takada, T. ;…

(Citation)
Osteoarthritis and Cartilage,30(3):481-493

(Issue Date)
2022-03

(Resource Type)
journal article

(Version)
Version of Record

Osteoarthritis and Cartilage 30 (2022) 481–493

Osteoarthritis and Cartilage

Involvement of autophagy in the maintenance of rat intervertebral disc homeostasis: an *in-vitro* and *in-vivo* RNA interference study of Atg5

R. Tsujimoto † [a], T. Yurube † [a] *, Y. Takeoka † [a], Y. Kanda †, K. Miyazaki †, H. Ohnishi †, Y. Kakiuchi †, S. Miyazaki †, Z. Zhang †, T. Takada ‡, R. Kuroda †, K. Kakutani †

† *Department of Orthopaedic Surgery, Kobe University Graduate School of Medicine, 7-5-1 Kusunoki-cho, Chuo-ku, Kobe, 650-0017, Japan*
‡ *Department of Orthopaedic Surgery, Kobe Hokuto Hospital, 37-3 Yamada-cho Shimotanigami Aza Umekidani, Kita-ku, Kobe, 651-1243, Japan*

ARTICLE INFO

Article history:
Received 25 May 2021
Accepted 19 December 2021

Keywords:
Intervertebral disc
Nucleus pulposus cells
Autophagy-related gene 5 (Atg5)
RNA interference (RNAi)
Rat tail temporary static compression model
Spine

SUMMARY

Objective: In the largest avascular low-nutrient intervertebral disc, resident cells would utilize autophagy, a stress-response survival mechanism by self-digestion and recycling wastes. Our goal was to elucidate the involvement of autophagy in disc homeostasis through RNA interference of autophagy-related gene 5 (Atg5).
Design: In vitro, small interfering RNAs (siRNAs) targeting autophagy-essential Atg5 were transfected into rat disc cells. Cell viability with levels of autophagy including Atg5 expression, apoptosis, and senescence was assessed under serum starvation and/or pro-inflammatory interleukin-1 beta (IL-1β) stimulation. *In vivo*, time-course autophagic flux was monitored following Alexa Fluor® 555-labeled Atg5-siRNA injection into rat tail discs. Furthermore, 24-h temporary static compression-induced disruption of Atg5 siRNA-injected discs was observed by radiography, histomorphology, and immunofluorescence.
Results: In disc cells, three different Atg5 siRNAs consistently suppressed autophagy with Atg5 protein knockdown (mean 44.4% [95% confidence interval: −51.7, −37.1], 51.5% [−80.5, −22.5], 62.3% [−96.6, −28.2]). Then, Atg5 knockdown reduced cell viability through apoptosis and senescence not in serum-supplemented medium (93.6% [−0.8, 21.4]) but in serum-deprived medium (66.4% [−29.8, −8.6]) further with IL-1β (44.5% [−36.9, −23.5]). In disc tissues, immunofluorescence detected intradiscal signals for the labeled siRNA even at 56-d post-injection. Immunoblotting found 56-d autophagy suppression with prolonged Atg5 knockdown (33.2% [−52.8, −5.3]). With compression, Atg5 siRNA-injected discs presented radiographic height loss ([−43.9, −0.8]), histological damage ([−5.5, −0.2]), and immunofluorescent apoptosis ([2.2, 22.2]) and senescence ([4.1, 19.9]) induction compared to control siRNA-injected discs at 56 d.
Conclusions: This loss-of-function study suggests Atg5-dependent autophagy-mediated anti-apoptosis and anti-senescence. Autophagy could be a molecular therapeutic target for degenerative disc disease.

Introduction

Back pain is a global health, workforce, and socioeconomic problem with a high lifetime prevalence of ~85%[1] and US medical expenditure of ~$100 billion/year[2]. Back pain has various causes, but intervertebral disc degeneration is a major independent factor[3]. The intervertebral disc is the largest avascular low-nutrient organ in the body, comprising the central nucleus pulposus (NP), surrounding annulus fibrosus (AF), and cartilaginous endplates[4]. During development, the AF arises from the mesenchyme[5], whereas the NP originates from the notochord[6]. In humans, disc-NP notochordal

* Address correspondence and reprint requests to: T. Yurube, Department of Orthopaedic Surgery, Kobe University Graduate School of Medicine, 7-5-1 Kusunoki-cho, Chuo-ku, Kobe, 650-0017, Japan. Tel: 81-78-382-5985; Fax: 81-78-351-6944.
E-mail addresses: tsujiryu1105@yahoo.co.jp (R. Tsujimoto), takayuru-0215@umin.ac.jp (T. Yurube), yoshiki_tkk@hotmail.com (Y. Takeoka), ykanda221@gmail.com (Y. Kanda), miya625819@gmail.com (K. Miyazaki), o0717ooo@yahoo.co.jp (H. Ohnishi), yuji_uz_7@yahoo.co.jp (Y. Kakiuchi), mghff229@yahoo.co.jp (S. Miyazaki), shouei76@hotmail.com (Z. Zhang), takada-t@hokuto-hp.or.jp (T. Takada), kurodar@med.kobe-u.ac.jp (R. Kuroda), kakutani@med.kobe-u.ac.jp (K. Kakutani).
[a] R.T., T.Y., and Y.T. contributed equally to this work.

https://doi.org/10.1016/j.joca.2021.12.004

cells exist only for the first 10 years[7], replaced by non-notochordal chondrocyte-like cells as the representation of a terminal differentiation stage of notochordal cells[8]. The disc's primary nutritional supply is diffusion through endplates. Endplate calcification reduces nutrient supply[9], resulting in cell decrease with apoptosis and senescence and extracellular matrix degradation[7,10]. Human disc degeneration begins in childhood with altered matrix composition[7,10]. Apoptosis, programmed cell death[11], increases in the disc with aging between 11 and 16 years old[7]. Senescence, irreversible cell cycle arrest[12], also increases with disc aging[13]. Therefore, there are possible links between apoptosis/senescence and notochordal cell disappearance/chondrocyte-like cell proliferation in the pathogenesis of disc degeneration.

Autophagy in the intervertebral disc has received increasing attention[14]. Autophagy, an intracellular clearance mechanism in which cells degrade and recycle their proteins and organelles, is involved in maintaining cell homeostasis under stressors including starvation and inflammation[15], and is negatively regulated by the mammalian target of rapamycin (mTOR) signaling pathway[16]. Autophagy includes autophagy-related (Atg) genes and proteins as key modulators, useful for monitoring this process[17]. Under typical physiological conditions, Atg protein expressions are relatively low and basal autophagy maintains cell homeostasis by decomposing waste products[18]. Meanwhile, under stress conditions, Atg proteins are activated, resulting in the formation and maturation of autophagosomes from phagophores, which capture damaged organelles, misfolded proteins, and impaired mitochondria in induced autophagy[15]. Autophagosomes fuse with lysosomes and are degraded by lysosome-derived enzymes with sequestered cellular components[15]. The autophagy-related gene 5 (Atg5), conjugated by Atg12, is present on the outer side of phagophores and essential for the elongation[17]. The light chain 3 (LC3), localized in the autophagosome membrane, is converted from cytosolic LC3-I to phosphatidylethanolamine-conjugated LC3-II by autophagy induction. Therefore, LC3-II is used as a marker of autophagosome formation and maturation[19]. The p62/sequestosome 1 (p62/SQSTM1) is a ubiquitin-binding protein, acting as a link between LC3 and ubiquitinated substrates[20]. The p62/SQSTM1 and p62/SQSTM1-bound polyubiquitinated proteins become incorporated into completed autophagosomes and are degraded in autolysosomes, which inversely correlate with autophagosome degradation[20]. This series of processes is called autophagic flux [Fig. 1(A)][21].

Although autophagy plays cytoprotective roles in various physiological processes and pathological events[15], autophagy involvement in intervertebral disc degeneration has not been fully clarified. Pharmacological inhibition would be simple to elucidate the autophagy function; however, its uncontaminated intracellular signaling blockade is difficult, leading to possible confounding effects[21]. Thus, RNA silencing is more suited to achieve specific autophagy suppression[21]. In this study, we targeted Atg5 as a key molecule in initiating autophagy, relatively specifically contributing to phagophore elongation[17]. Because of the disc's anatomical, biochemical, and nutritional characteristics, we hypothesized that autophagy would serve for the maintenance of disc homeostasis. To clarify the autophagy involvement, we designed an *in-vitro* and *in-vivo* loss-of-function study of autophagy using the RNA interference (RNAi) technique against autophagy-essential Atg5 in rat disc cells and tissues.

Materials and methods

Ethics statement

All experimental procedures were performed in accordance with the Institutional Animal Care and Use Committee (P140609 and P190709) at Kobe University Graduate School of Medicine.

Antibodies and reagents

The antibodies and reagents used are listed in Supplemental Table 1.

Cells

Sixty-two 12-week-old male Sprague–Dawley rats (mean 476.6 g [95% confidence interval (CI): 471.7, 481.5]) purchased from CLEA Japan (Tokyo, Japan) were randomly applied to *in-vitro* and *in-vivo* experiments without exclusions. Coccygeal (C) discs from 20 rats (475.4 g [464.2, 486.5]) were dissected into the NP and AF after euthanasia. Rat disc NP tissues were digested in 1% penicillin/streptomycin-supplemented Dulbecco's modified Eagle's medium (DMEM) with 10% fetal bovine serum (FBS) and 0.114% collagenase type 2 for 1 h at 37°C. Isolated disc NP cells were grown to ~80% confluence as a monolayer in DMEM with 10% FBS under 2% O_2 at 37°C[9]. To retain the phenotype, only first-passage cells were used for evaluation[22–25].

The density of randomly distributed seeding cells ($n = 20$) was 5.0×10^3/well (96-well plate) for viability, 1.5×10^5/well (6-well plate) for protein extraction, and 1.2×10^4/well (8-well chamber) for staining. In respective experiments, 4 cell samples from 4 different animals (each $n = 4$) were tested based on not a priori sample-size calculation but literature[22–25].

After 24-h RNAi treatment in 10% FBS-supplemented DMEM, cells were applied to Western blotting (WB) for disc NP phenotype, Atg5 knockdown, and autophagy. Additionally, to simulate clinically relevant disease conditions of serum deprivation and/or inflammation, cells were cultured for 24 h in DMEM with 10% FBS, with serum-free 0% FBS, or with 0% FBS and 10-ng/ml interleukin-1 beta (IL-1β), a pro-inflammatory cytokine linked to the pathogenesis and severity of disc degeneration[26]. Then, cell viability was assessed using the Cell Counting Kit-8 (CCK-8). Cell count was performed. Immunoblotting for matrix anabolism, apoptosis, and senescence, apoptotic terminal deoxynucleotidyl transferase dUTP nick end labeling (TUNEL) staining, senescence-associated beta-galactosidase (SA-β-gal) staining, and immunofluorescence for autophagy, apoptosis, and senescence were conducted [Fig. 1(B)].

Animals and surgical procedures

Forty-two rats (477.1 g [471.3, 482.9]) were used. To confirm *in-vivo* transfection in rat tails ($n = 18$), control and Alexa Fluor® 555-labeled Atg5 small interfering RNA (siRNA)–Invivofectamine™ 3.0 reagent complexes were injected into C8–C9 and C11–C12 discs and C9–C10 and C12–C13 discs, respectively. Under general anesthesia, 2-μl solution was injected using a 33-gauge needle at the disc center through a 5-mm longitudinal skin incision[27,28]. At 2–56 d, C8–C9 control siRNA-injected and C9–C10 Atg5 siRNA-injected disc and C11–C12 control siRNA-injected and C12–C13 Atg5 siRNA-injected disc tissues were acquired and analyzed by immunofluorescence for Alexa Fluor® 555-labeled Atg5-siRNA transfection and WB for Atg5 knockdown and autophagy, respectively [Fig. 1(C)].

A rat tail temporary static compression model was used to reproduce mechanical stress-induced disc degenerative changes[29–33]. Under general anesthesia, an Ilizarov-type apparatus with springs was attached between C8 and C10 vertebrae of rat tails ($n = 24$). Control and Atg5 siRNA–Invivofectamine™ 3.0 reagent complexes were injected into C8–C9 and C11–C12 discs and C9–C10 and C12–C13 discs, respectively. Then, 1.3-MPa axial force, corresponding to a disc loading force produced by lifting a moderate weight in the human lumbar spine[34], was applied to C8–C9 and C9–C10 discs for 24 h and subsequently released. At 0–56 d,

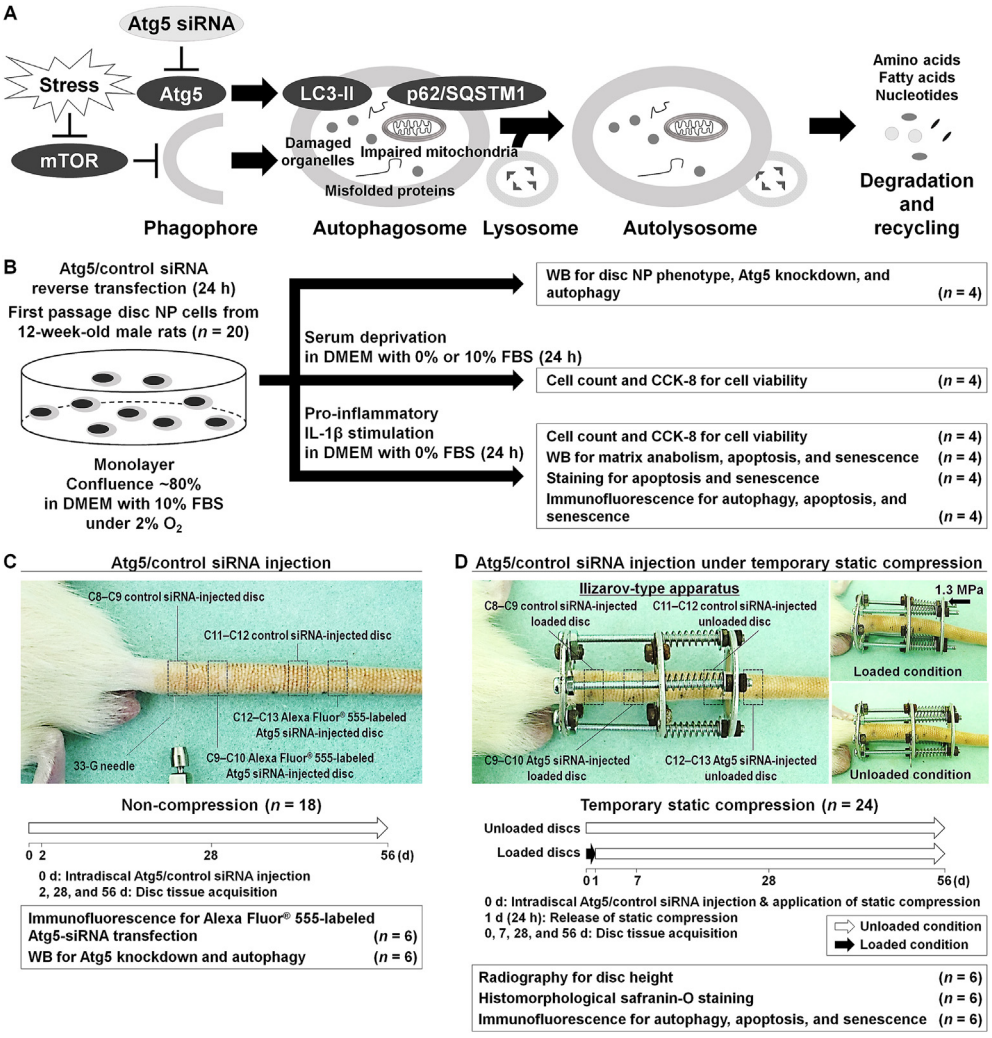

Fig. 1

Osteoarthritis and Cartilage

Schematic illustration of disc cellular autophagy and *in-vitro* and *in-vivo* experimental regimens. (A) Schematic illustration of autophagic flux. Under stress conditions, mTOR is suppressed, which initiates autophagy through the activation of autophagy-related genes. The Atg5 is an autophagy-essential factor for phagophore elongation and autophagosome formation, which is driven by LC3-II. The p62/SQSTM1 and p62/SQSTM1-bound polyubiquitinated proteins become incorporated into the completed autophagosome. It fuses with the lysosome to form the autolysosome, where the enclosed contents are degraded and recycled. To suppress autophagy, post-transcriptional gene silencing using siRNAs against Atg5 was used. (B) Schematic illustration of the *in-vitro* study design and sample number. First passage, ~80%-confluent, monolayer disc NP cells from 12-week-old male rats ($n = 20$) were reverse transfected with siRNAs targeting Atg5 or non-specific control in DMEM with 10% FBS under 2% O_2 for 24 h and analyzed by WB for the phenotype, Atg5 knockdown, and autophagy ($n = 4$); by cell count and CCK-8 for cell viability after 24-h serum deprivation in DMEM with 0% or 10% FBS ($n = 4$); by cell count, CCK-8 for cell viability, WB for matrix anabolism, apoptosis, and senescence, staining for apoptosis and senescence, and immunofluorescence for autophagy, apoptosis, and senescence after 24-h serum withdrawal and pro-inflammatory stimulation in DMEM with 0% FBS and 10-ng/ml IL-1β (each $n = 4$). (C) Schematic illustration of the *in-vivo* siRNA transfection study design and sample number. In rat tails ($n = 18$), control siRNA was injected using a 33-gauge needle into C8–C9 and C11–C12 discs, while Alexa Fluor® 555-labeled Atg5 siRNA was injected into C9–C10 and C12–C13 discs. At 2–56 d, tissues of C8–C9 control siRNA-injected and C9–C10 Atg5 siRNA-injected discs and C11–C12 control siRNA-injected and C12–C13 Atg5 siRNA-injected discs were acquired and analyzed by immunofluorescence for Alexa Fluor® 555-labeled Atg5-siRNA transfection and WB for Atg5 knockdown and autophagy, respectively ($n = 6$/time point). (D) Schematic illustration of the *in-vivo* temporary static compression study design and sample number. In rat tails ($n = 24$), an Ilizarov-type apparatus with springs was affixed between C8 and C10. Control siRNA was injected into C8–C9 and C11–C12 discs, whereas Atg5 siRNA was injected into C9–C10 and C12–C13 discs. Then, 1.3-MPa axial force was applied to C8–C9 and C9–C10 discs for 24 h and subsequently released. At 0–56 d, tissues of C8–C9 control siRNA-injected loaded, C9–C10 Atg5 siRNA-injected loaded, C11–C12 control siRNA-injected unloaded, and C12–C13 Atg5 siRNA-injected unloaded discs were acquired following radiography for the height and analyzed by histomorphological safranin-O staining and immunofluorescence for autophagy, apoptosis, and senescence ($n = 6$/time point).

C8–C9 control siRNA-injected loaded, C9–C10 Atg5 siRNA-injected loaded, C11–C12 control siRNA-injected unloaded, and C12–C13 Atg5 siRNA-injected unloaded disc tissues were acquired after radiographic imaging for the height and analyzed by histomorphological safranin-O staining and immunofluorescence for autophagy, apoptosis, and senescence [Fig. 1(D)].

Sample size ($n = 6$/time point) was based on literature[27–33] but not a priori sample-size calculation. Rats were fed separately in a specific pathogen-free housing cage with freely available food and water. The room had a controlled 12-h light/dark cycle, temperature (23 ± 2°C), and humidity (55 ± 5%). Humane endpoints, e.g., ≥20% weight loss and behavioral changes, were determined.

RNAi

The RNAi was performed using small interfering RNAs (siRNAs) to knockdown Atg5 with the reverse transfection method, allowing high transfection efficiency[35]. *In vitro*, three different Atg5 siRNAs [Supplemental Table 2] were used to exclude off-target effects. A non-targeting siRNA was used as a negative control. Cells in 10% FBS-supplemented DMEM were added to each siRNA with Lipofectamine™ RNAiMAX transfection reagent diluted in Opti-Minimal Essential Medium I and then cultured for 24 h. Applied amounts of siRNAs were 60 (6-well plate), 4.8 (8-well chamber), and 2 (96-well plate) pmol/well.

In vivo, Atg5 or control siRNA with Invivofectamine™ 3.0 reagent (final 1.5-pmol/l concentration) was prepared. The Alexa Fluor® 555-labeled Atg5 siRNA was used to assess successful tissue transfection.

Cell viability assay

In vitro, cell viability was assessed by CCK-8 dehydrogenase activity, the absorbance of which (450 nm) was measured using the Model 680 microplate reader. In addition, images were photographed with the BZ-X700 microscope. The number of adherent cells was counted in duplicated four random low-power fields (× 100) (LPFs) using the ImageJ software (https://imagej.nih.gov/ij/).

Protein extraction, sodium dodecyl sulfate (SDS)–polyacrylamide gel electrophoresis (PAGE), and WB

Cells were scraped off on ice in 3-(*N*-morpholino)propanesulfonic acid buffer containing protease and phosphatase inhibitors. Harvested tissues were homogenized using the MS-100R bead-beating disrupter for 30 s twice at 4°C in the T-PER™ tissue protein extraction reagent with protease and phosphatase inhibitors. Soluble proteins were collected after 20,000-×*g* centrifugation for 15 min at 4°C. Samples were stored at −80°C. Protein concentration was determined by the bicinchoninic acid assay.

Equal 30-μg amounts of protein were mixed with the SDS–PAGE sample buffer, boiled for 5 min, and resolved on a 7.5–15.0% polyacrylamide gel. Separated proteins in the tris(hydroxymethyl) aminomethane–glycine–SDS buffer system were transblotted to a polyvinylidene difluoride membrane and probed with primary antibodies for 12 h at 4°C (1:200–1:1,000 dilution) followed by secondary antibodies (1:400 dilution) for 1 h at room temperature. Signals were visualized by enhanced chemiluminescence. Images were obtained using the Chemilumino analyzer LAS-3000 mini. Band intensity was quantified using ImageJ.

In vitro and *in vivo*, WB was designed to analyze intracellular expression of disc NP notochord-related brachyury and CD24[36], matrix anabolism-related aggrecan and collagen type II alpha 1 (Col2a1)[10], autophagy-related Atg5, LC3, and p62/SQSTM1[21], apoptosis-related poly (ADP-ribose) polymerase (PARP) and cleaved caspase-9[11], senescence-related p53, p21/CIP1, and p16/INK4a[12] in total cell or tissue protein extracts. Protein expression was normalized to loading control tubulin and shown as the relative percentage of control.

Paraffin-embedded tissue preparation

In vivo, functional rat caudal spinal units (vertebral body–disc–vertebral body) were obtained after euthanasia, 1-d fixed en-bloc with 4% paraformaldehyde, 7-d decalcified in 10% ethylenediaminetetraacetic acid, embedded in paraffin, and cut mid-sagittal into 7-μm sections for histomorphology and immunofluorescence.

TUNEL staining

In vitro, cells were fixed with 4% paraformaldehyde for 10 min and applied to fluorescein-labeled TUNEL staining for apoptotic fragmented DNA detection with 4',6-diamidino-2-phenylindole (DAPI) for counterstaining[37]. *In vivo*, apoptotic TUNEL positivity in tissue sections was examined. Under the BZ-X700 microscope and ImageJ, the percentage of TUNEL-positive cells was calculated relative to the total number of DAPI-positive cells in duplicated four random LPFs.

SA-β-gal staining

In vitro, senescent cells were identified by cytochemical SA-β-gal staining at pH 6.0[38]. The percentage of SA-β-gal-positive cells was calculated in duplicated four random LPFs.

Immunofluorescence

In vitro and *in vivo*, multi-color immunofluorescence was performed to understand disc cellular relationship between autophagy, apoptosis, and senescence. After antigen-retrieval, permeabilization, and blocking, fixed cells and disc tissue sections were incubated with autophagic Atg5[17] and senescent p16/INK4a[39] primary antibodies (both 1:100 dilution) and apoptotic fluorescein-labeled TUNEL[37] for 12 h at 4°C and subsequently with Alexa Fluor® 568 and 647 secondary antibodies (1:200 dilution) and DAPI for 1 h at room temperature. The percentage of Atg5-positive cells, TUNEL-positive cells, and p16/INK4a-positive cells was calculated relative to DAPI-positive cells in duplicated four random LPFs.

In vivo, immunofluorescence for Alexa Fluor® 555-labeled Atg5 siRNA and DAPI was performed to disclose the efficacy and working period of intradiscal transfection. The Alexa Fluor® 555 signals are detectable only under the presence of Atg5 siRNAs incorporated in cells.

Radiography

In vivo, lateral radiographs were taken using a VPX-30E system and IXFR film (exposure time, 40 s; distance, 40 cm; current, 3 mA; voltage, 35 kV). Disc height was measured using ImageJ twice at a 1-week interval by each of two investigators blinded to this study, normalized to adjacent vertebral body heights as the disc height index (DHI), shown as the percent of preoperative DHI (% DHI = [postoperative DHI/preoperative DHI] × 100), and further normalized to the intact disc as the normalized %DHI (normalized % DHI = [experimental %DHI/intact %DHI] × 100)[40].

Histomorphology

In vivo, safranin-O, fast green, and hematoxylin staining was performed to demonstrate disc tissue morphological disruption.

Histopathological grade, from 0 (non-degenerated) to 16 (severely degenerated) for NP morphology, NP cellularity, NP–AF border, AF morphology, and endplate[41], was assessed in duplicate twice at a 1-week interval by each of two blinded investigators, and the median scores were used for evaluation.

Statistical analysis

Data are presented as the mean [95% CI: lower limit, upper limit] in the text and dot and box plots in the graphs. With the normality assumption, one-way repeated measured analysis of variance (ANOVA), two-way ANOVA, and three-way ANOVA with the Tukey–Kramer post-hoc test were used to assess effects of "treatment", "experimental condition", and "time" on *in-vitro* cell viability, cell count, WB, TUNEL staining, SA-β-gal staining, and immunofluorescence, on *in-vivo* WB, and on *in-vivo* radiography, histomorphology, and immunofluorescence, respectively. The intra-class correlation coefficient was calculated to determine the intra-observer and inter-observer reliability for radiography and histology. Statistical analysis was performed using IBM SPSS Statistics 23.0 (IBM, Armonk, NY).

Results

In-vitro Atg5 knockdown suppresses autophagy and promotes apoptosis and senescence in rat disc NP cells

First, notochordal marker expression was evaluated to validate rat disc NP phenotype. In WB, protein extracts from tested samples all showed positive expression of notochord-related brachyury and CD24 [Fig. 2(A)]. Then, we assessed whether Atg5 RNAi using three different siRNAs could effectively knockdown the corresponding protein. Significant decrease in Atg5 expression was seen following every Atg5-siRNA transfection (sequence 1, mean 44.4% knockdown [95% CI: −51.7, −37.1]; sequence 2, 51.5% knockdown [−80.5, −22.5]; sequence 3, 62.3% knockdown [−96.6, −28.2]) [Fig. 2(A)]. Furthermore, we assessed Atg5-RNAi effects on autophagy. Immunoblotting demonstrated that Atg5-siRNA treatment decreased LC3-II (sequence 1, 62.1% [−64.5, −11.3]; sequence 2, 64.0% [−62.6, −9.5]; sequence 3, 48.3% [−78.3, −25.2]) and increased p62/SQSTM1 (sequence 1, 170.5% [33.7, 107.3]; sequence 2, 169.4% [32.6, 106.2]; sequence 3, 188.0% [51.2, 124.8]) [Fig. 2(A)], both indicating successful Atg5 knockdown-mediated autophagy suppression. In subsequent experiments, the sequence-3 Atg5 siRNA with the highest knockdown efficiency was used.

Second, to understand Atg5 RNAi-modified disc cellular physiology, we assessed cell viability by CCK-8 and counted cell number. These were not significantly different between the groups treated by control and Atg5 siRNAs in 10% FBS-supplemented DMEM (CCK-8, 100.0% vs 93.6% [−0.8, 21.4]; cell number, 132.3/LPF vs 127.3/LPF [−16.5, 6.5]) but significantly decreased with Atg5 knockdown under autophagy-requiring conditions in serum-free DMEM (CCK-8, 77.4% vs 66.4% [−29.8, −8.6]; cell number, 84.8/LPF vs 71.8/LPF [−24.5, −1.5]) and further with IL-1β supplementation (CCK-8, 56.7% vs 44.5% [−36.9, −23.5]; cell number, 49.5/LPF vs 33.0/LPF [−28.0, −5.0]), indicating Atg5 knockdown-dependent and serum withdrawal and inflammation-dependent decrease in cell number and viability [Fig. 2(B)].

Third, we assessed Atg5-RNAi effects on disc cellular matrix anabolism, apoptosis, and senescence. Pro-inflammatory IL-1β stimulation resulted in downregulation of anabolic aggrecan ([−49.8, −16.6]) and Col2a1 ([−53.8, −27.6]) protein expression, which was further enhanced by Atg5 RNAi (Col2a1, [−26.1, −0.3]). Then, IL-1β stimulation induced significant downregulation of apoptosis-related PARP ([−31.4, −7.5]) and significant upregulation of apoptotic cleaved PARP ([17.3, 69.2]) and cleaved caspase-9 ([12.5, 52.6]) and senescent p21/CIP1 ([19.7, 103.1]) and p16/INK4a ([11.5, 34.6]) expression. Furthermore, Atg5 knockdown additionally increased IL-1β-induced markers of apoptosis and senescence compared with Atg5 siRNA-treated IL-1β-unstimulated cells (PARP, [−39.7, −15.7]; cleaved PARP, [12.3, 64.3]; cleaved caspase-9, [22.3, 62.4]; p53, [38.1, 156.8]; p21/CIP1, [24.2, 107.6]; p16/INK4a, [14.8, 37.9]) and control siRNA-treated IL-1β-stimulated cells (cleaved PARP, [6.2, 58.1]; cleaved caspase-9, [0.5, 40.6]; p53, [10.1, 128.8]; p16/INK4a, [5.7, 28.8]) [Fig. 2(C)]. These data suggest accelerated apoptosis and senescence by Atg5 knockdown under stressful serum deprivation and inflammation.

In-vitro Atg5 knockdown increases the incidence of apoptosis and senescence in rat disc NP cells

In-vitro Atg5-RNAi effects on disc cellular apoptosis and senescence were further evaluated by TUNEL staining, SA-β-gal staining, and multi-color immunofluorescence. The percentage of TUNEL-positive cells increased following IL-1β stimulation ([95% CI: 15.8, 33.2]), amplified by Atg5 RNAi ([0.4, 22.9]) [Fig. 3(A)]. Also, SA-β-gal-positive cell percentage increased with IL-1β supplementation ([13.3, 29.5]), exaggerated by Atg5 RNAi ([1.6, 17.8]) [Fig. 3(B)]. Then, Atg5 RNAi significantly decreased immunopositivity for Atg5 in IL-1β-unstimulated ([−62.0, −40.7]) and IL-1β-stimulated ([−57.2, −35.9]) cells, which contrastingly increased the percentage of TUNEL-positive ([1.1, 29.2]) and p16/INK4a-positive ([0.1, 15.8]) cells under IL-1β stimulation. However, immunopositivity for apoptotic TUNEL and senescent p16/INK4a remained overlapped partially (3.7–17.0%) [Fig. 3(C)]. These results support promoted apoptosis and senescence by Atg5 knockdown.

In-vivo Atg5 knockdown facilitates prolonged suppression of autophagy in rat disc NP tissues

Based on the *in-vitro* disc cytotoxic effects of Atg5 knockdown, *in-vivo* intradiscal gene-silencing experiments using Atg5 RNAi were designed. All rats underwent surgery well and gained body weight throughout the experiment (mean 584.7 g, [95% CI: 577.6, 591.9] at 56 d). All springs maintained their compressive length and fully recovered after release, indicating sustained axial loading. There were no signs of infection, skin necrosis, or neurological problems.

To corroborate local siRNA introduction into rat tail discs and uptake by NP cells, Alexa Fluor® 555-labeled Atg5 siRNA was used. Successful administration was confirmed by radiography upon injecting a contrast agent [Fig. 4(A)]. Technically in this system, only siRNAs incorporated into the cytoplasm are detectable. Immunofluorescence showed the red signal for labeled Atg5 siRNA in the disc NP-cell cytoplasm 2–56 d after injection, supporting successful Atg5-siRNA transfection into disc NP cells and a long-term 56-d maintenance [Fig. 4(B)]. Immunoblotting displayed sustained Atg5 protein downregulation in Atg5 siRNA-injected discs (2 d, 45.0% knockdown [−66.3, −19.9]; 28 d, 36.9% knockdown [−56.4, −10.0]; 56 d, 33.2% knockdown [−52.8, −5.3]) [Fig. 4(C)]. Furthermore, Atg5 RNAi-mediated prolonged autophagy suppression was observed with decreased LC3-II (2 d, 61.4% [−59.0, −14.6]; 28 d, 64.4% [−54.1, −9.8]; 56 d, 60.6% [−56.9, −12.5]) and increased p62/SQSTM1 (2 d, 139.1% [16.9 65.0]; 28 d, 131.9% [11.5, 59.6]; 56 d,

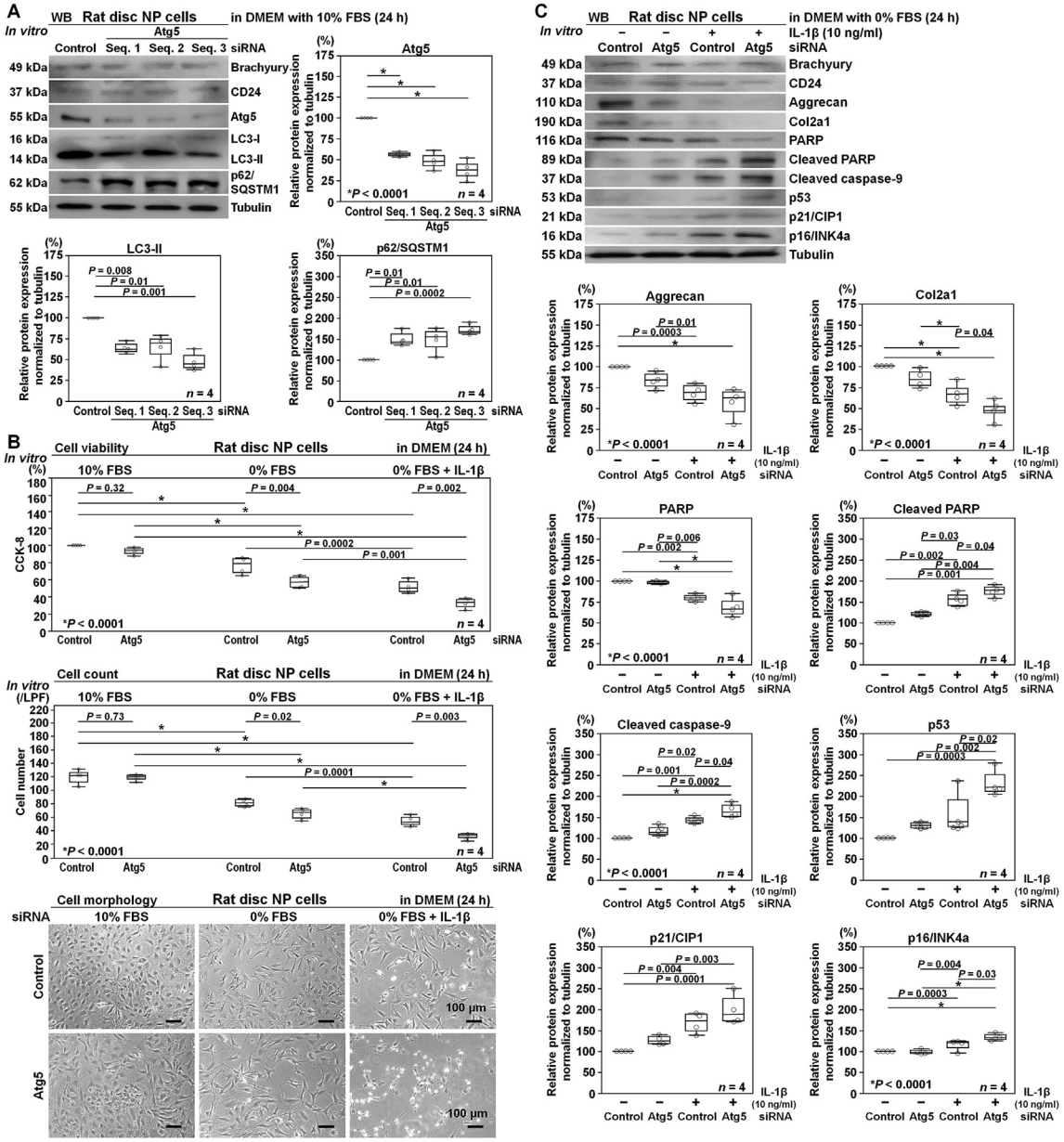

Fig. 2

Osteoarthritis and Cartilage

***In-vitro* Atg5 knockdown suppresses autophagy and promotes apoptosis and senescence in rat disc NP cells.** (A) WB for phenotypic brachyury and CD24, autophagic Atg5, LC3, and p62/SQSTM1, and loading control tubulin of total protein extracts from rat disc NP cells after Atg5 or control siRNA transfection in DMEM with 10% FBS for 24 h. Changes in relative protein expression of Atg5, LC3-II, and p62/SQSTM1 normalized to tubulin are shown. (B) Changes in CCK-8-based viability, counting number, and morphological appearance of rat disc NP cells after Atg5 or control siRNA transfection in DMEM with 10% FBS for 24 h followed by in DMEM with 10% FBS, with 0% FBS, or with 0% FBS and 10-ng/ml IL-1β for 24 h. Cell count was performed in respective four random LPFs of duplicates. (C) WB for phenotypic brachyury and CD24, anabolic aggrecan and Col2a1, apoptotic PARP, cleaved PARP, and cleaved caspase-9, senescent p53, p21/CIP1, and p16/INK4a, and loading control tubulin of total protein extracts from rat disc NP cells after Atg5 or control siRNA transfection in DMEM with 10% FBS for 24 h followed by in DMEM with 0% FBS and 10-ng/ml IL-1β for 24 h. Changes in relative protein expression of aggrecan, Col2a1, PARP, cleaved PARP, cleaved caspase-9, p53, p21/CIP1, and p16/INK4a normalized to tubulin are shown. In (A), (B), and (C), data are presented with dot and box plots ($n = 4$). One-way repeated measures ANOVA with the Tukey–Kramer post-hoc test was used. Immunoblots and cellular images shown are representative of experiments with similar results.

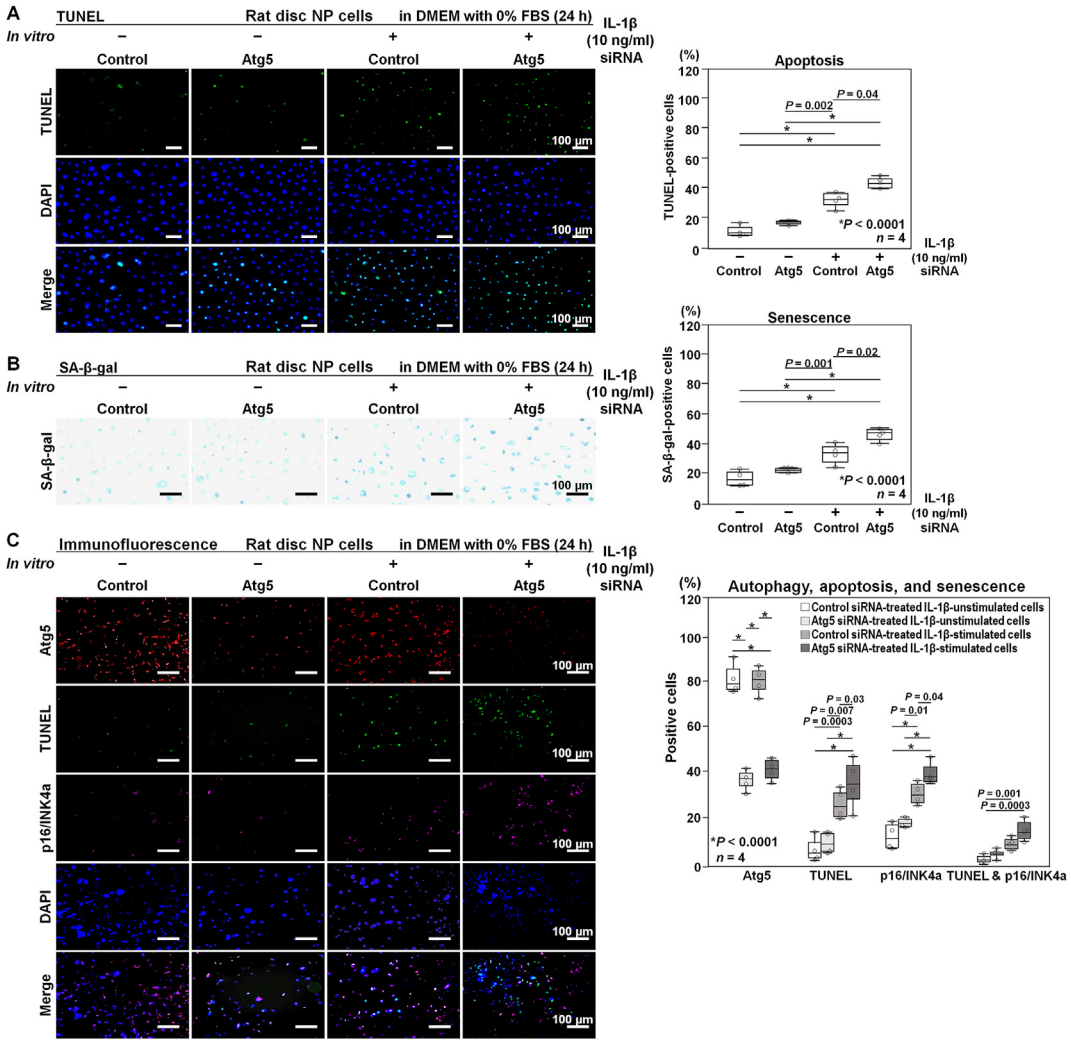

Fig. 3

Osteoarthritis and Cartilage

***In-vitro* Atg5 knockdown increases the incidence of apoptosis and senescence in rat disc NP cells.** (A) Immunofluorescence for apoptotic TUNEL (green), nuclear DAPI (blue), and merged signals of rat disc NP cells after Atg5 or control siRNA transfection in DMEM with 10% FBS for 24 h followed by in DMEM with 0% FBS and 10-ng/ml IL-1β for 24 h. Changes in the percentage of TUNEL-positive cells relative to DAPI-positive cells are shown. (B) SA-β-gal staining of rat disc NP cells after Atg5 or control siRNA transfection in DMEM with 10% FBS for 24 h followed by in DMEM with 0% FBS and 10-ng/ml IL-1β for 24 h. Changes in the percentage of SA-β-gal-positive cells relative to total cells are shown. (C) Immunofluorescence for autophagic Atg5 (red), apoptotic TUNEL (green), senescent p16/INK4a (purple), nuclear DAPI (blue), and merged signals of rat disc NP cells after Atg5 or control siRNA transfection in DMEM with 10% FBS for 24 h followed by in DMEM with 0% FBS and 10-ng/ml IL-1β for 24 h. Changes in the percentage of Atg5-positive, TUNEL-positive, p16/INK4a-positive, and TUNEL and p16/INK4a-co-positive cells relative to DAPI-positive cells are shown. In (A), (B), and (C), cell count was performed in respective four random LPFs of duplicates. Data are presented with dot and box plots ($n = 4$). One-way repeated measures ANOVA with the Tukey–Kramer post-hoc test was used. Immunofluorescent and cytochemical images shown are representative of experiments with similar results.

124.2% [4.8, 52.9]) [Fig. 4(C)]. These findings indicate extended intradiscal autophagy suppression after Atg5 knockdown.

In-vivo Atg5 knockdown advances radiographic and histomorphological disc disruption under temporary static compression in rats

In-vivo Atg5-RNAi effects on disc tissue disruption were evaluated under temporary static compression. Radiographic %DHI analysis exhibited the intra-observer reliability of 0.949–0.978 and inter-observer reliability of 0.901, indicating an acceptable reproducibility. In Atg5 siRNA-injected loaded discs, %DHI was significantly lower compared with Atg5 siRNA-injected unloaded discs (7 d, [95% CI: −23.1, −5.3]; 28 d, [−41.5, −15.5]; 56 d, [−65.4, −20.6]) and control siRNA-injected loaded discs (7 d, [−19.3, −1.4]; 28 d, [−36.3, −10.2]; 56 d, [−43.9, −0.8]), demonstrating the progressive loss between 7 d ([−49.8, −26.0]) and 28 d ([−33.6, −9.7]) vs 56 d [Fig. 5(A)]. These findings suggest an involvement of Atg5-dependent autophagy in maintaining disc height against mechanical loading.

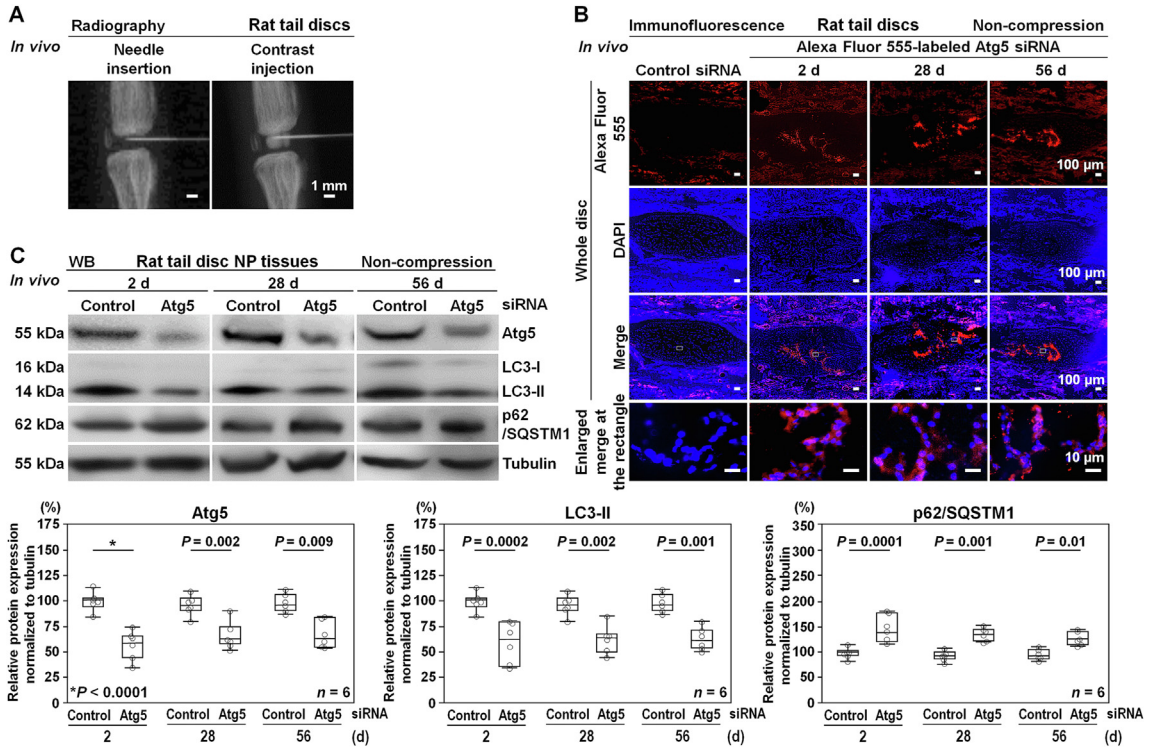

Fig. 4

Osteoarthritis and Cartilage

***In-vivo* Atg5 knockdown facilitates prolonged suppression of autophagy in rat disc NP tissues.** (A) Confirmation with radiography of successful intradiscal 33-gauge needle insertion and 2-μl contrast injection. (B) Immunofluorescence for Alexa Fluor® 555-labeled autophagic Atg5 siRNA (red), nuclear DAPI (blue), and merged signals of rat tail discs at 2, 28, and 56 d after Alexa Fluor® 555-labeled Atg5 or control siRNA injection. White rectangles indicate the disc NP area shown as the enlarged merged images. (C) WB for autophagic Atg5, LC3, and p62/SQSTM1 and loading control tubulin of total protein extracts from rat tail disc NP tissues at 2, 28, and 56 d after Atg5 or control siRNA injection. Changes in relative protein expression of Atg5, LC3-II, and p62/SQSTM1 normalized to tubulin are shown. In (C), data are presented with dot and box plots ($n = 6$). Two-way ANOVA with the Tukey–Kramer post-hoc test was used. Immunofluorescent images and immunoblots shown are representative of experiments with similar results.

Histological grading illustrated the intra-observer reliability of 0.943–0.968 and inter-observer reliability of 0.916, suggesting an appropriate reproducibility. Safranin-O staining presented significantly higher degenerative scores in Atg5 siRNA-injected loaded discs than Atg5 siRNA-injected unloaded discs (28 d, [−7.7, −2.6]; 56 d, [−10.3, −5.0]) and control siRNA-injected loaded discs (56 d, [−5.5, −0.2]). While Atg5 siRNA-injected unloaded discs showed no significant histopathological changes to control siRNA-injected unloaded discs, NP-cell clustering, matrix condensation, and AF disorganization were remarkable in Atg5 siRNA-injected loaded discs at 56 d [Fig. 5(B), Supplemental Table 3], suggesting a contribution of Atg5-dependent autophagy to disc tissue maintenance under mechanical stress.

In-vivo Atg5 knockdown enhances immunofluorescent apoptosis and senescence under temporary static compression in rats

We finally performed multi-color immunofluorescence for autophagic Atg5, apoptotic TUNEL, and senescent p16/INK4a in this model. Immunopositivity for Atg5 was significantly lower in Atg5 siRNA-injected discs than control siRNA-injected ones under unloaded (7 d, [95% CI: −56.6, −28.4]; 28 d, [−46.3, −33.1]; 56 d, [−58.2, −16.8]) and loaded conditions (7 d, [−55.6, −30.3]; 28 d, [−61.1, −33.5]; 56 d, [−56.7, −18.9]) In Atg5 siRNA-injected loaded discs, the percentage of TUNEL-positive (7 d, [27.8, 45.8]; 28 d, [34.4, 54.9]; 56 d, [27.0, 45.9]) and p16/INK4a-positive (7 d, [23.9, 39.1]; 28 d, [35.3, 50.6]; 56 d, [27.6, 43.5]) cells was both significantly higher than Atg5 siRNA-injected unloaded discs and control siRNA-injected loaded discs at 56 d (TUNEL, [2.2, 22.2]; p16/INK4a, [4.1, 19.9]). In Atg5 siRNA-injected unloaded discs, the percentage of TUNEL-positive and p16/INK4a-positive cells was not significantly different from control siRNA-injected unloaded discs. Similar to the *in-vitro* finding, *in-vivo* co-immunopositivity for apoptotic TUNEL and senescent p16/INK4a was relatively limited (7 d, 1.6–9.8%; 28 d, 2.2–15.0%; 56 d, 3.7–17.0%) [Fig. 6]. Collectively, the observed findings support anti-apoptosis and anti-senescence as a consistent role of Atg5-dependent autophagy in intervertebral disc homeostasis.

Discussion

This is the first study showing progressive disc degenerative changes induced by *in-vitro* and *in-vivo* Atg5 RNAi-mediated autophagy suppression. *In vitro*, successful autophagy suppression

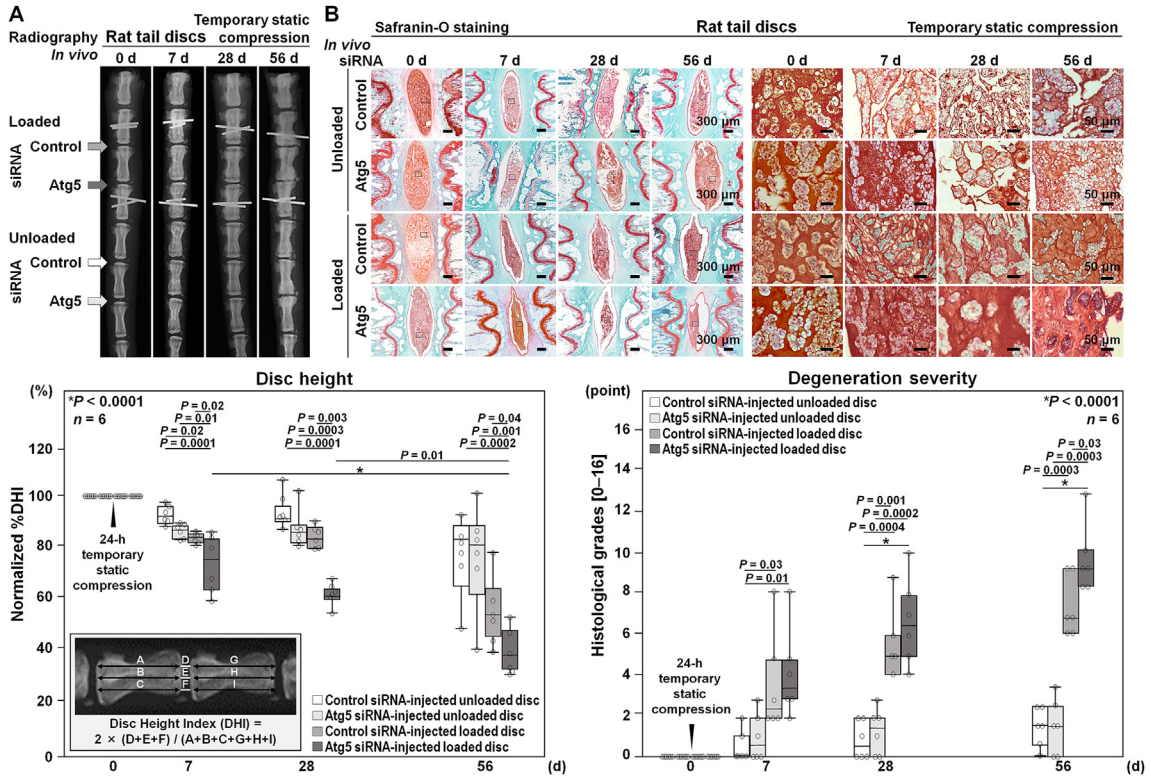

Fig. 5

Osteoarthritis and Cartilage

***In-vivo* Atg5 knockdown advances radiographic and histomorphological disc disruption under temporary static compression in rats.** (A) Lateral radiographs of rat tail C11–C12 control siRNA-injected unloaded (white arrow), C12–C13 Atg5 siRNA-injected unloaded (light-gray arrow), C8–C9 control siRNA-injected loaded (intermediate-gray arrow), and C9–C10 Atg5 siRNA-injected loaded (dark-gray arrow) discs at 0, 7, 28, and 56 d under temporary static compression at 1.3 MPa for 24 h. Changes in the height of control siRNA-injected unloaded, Atg5 siRNA-injected unloaded, control siRNA-injected loaded, and Atg5 siRNA-injected loaded discs are shown. (B) Safranin-O staining of rat tail C11–C12 control siRNA-injected unloaded, C12–C13 Atg5 siRNA-injected unloaded, C8–C9 control siRNA-injected loaded, and C9–C10 Atg5 siRNA-injected loaded discs at 0, 7, 28, and 56 d under temporary static compression at 1.3 MPa for 24 h. Changes in the histopathological grade of control siRNA-injected unloaded, Atg5 siRNA-injected unloaded, control siRNA-injected loaded, and Atg5 siRNA-injected loaded discs are shown. In (A) and (B), data are presented with dot and box plots ($n = 6$). Three-way ANOVA with the Tukey–Kramer post-hoc test was used. Radiographs and histomorphological images shown are representative of experiments with similar results.

was confirmed by introducing siRNA targeting Atg5, an essential autophagy factor, into rat disc NP cells. This is consistent with human disc NP-cell findings, undergoing Atg5 downregulation[25]. The observed knockdown efficiency of Atg5 siRNAs is comparable with literature (46–98%)[35]. Following Atg5 RNAi, apoptosis and senescence rates increased in cells under serum deprivation, further promoting after pro-inflammatory IL-1β stimulation. These anti-apoptotic and anti-senescent findings of Atg5-dependent autophagy in rat disc NP cells are consistent with human articular chondrocytes exhibiting enhanced apoptosis and senescence by Atg5 RNAi[42]. Since autophagy is negatively regulated by mTOR signaling[16], we previously reported autophagy induction by silencing mTOR complex 1 (mTORC1)[22] and administrating temsirolimus, an mTORC1 inhibitor[23], in human disc NP cells. Selective mTORC1 inhibition activated autophagy with anti-apoptosis and anti-senescence. However, Akt, located upstream of mTORC1 to promote cell survival by suppressing apoptosis[16], was also activated through the negative feedback loop[16]. Therefore, mTORC1 inhibition-mediated cytoprotection cannot completely exclude Akt activation effects. This study shows that specific autophagy suppression through Atg5 knockdown increases apoptosis and senescence in rat disc NP cells, suggesting an anti-apoptotic and anti-senescent contribution of Atg5-dependent autophagy to the homeostasis maintenance.

In vivo, Atg5 siRNA was found within the disc NP through 56-d post-injection. The observed knockdown efficiency of Atg5 siRNA locally administered in rat disc NP tissues is comparable with that in other tissues, e.g., brain, eye, and skin (10–75%)[43]. Furthermore, 56-d intradiscal autophagy suppression was confirmed, suggesting a long-term stability and capability of siRNA to block intradiscal protein expression without being metabolized. In other organs, local siRNA administration effects are maintained as short as 1–16-d[43]. Meanwhile, the reported siRNA-retaining period in rat disc NP cells and tissues was 2–3 weeks[44] and ≥24 weeks[28]. This notable feature could be due to the anatomical (avascular, encapsulated) and biological (highly differentiated, slow proliferated) characteristics of the disc[27,28]. Thus, we regard siRNAs as a potent tool for local gene therapy in disc disease. Since high effectiveness and long-term efficacy are advantages of gene therapy[45], single administration might provide sufficient therapeutic effects in future clinical practice.

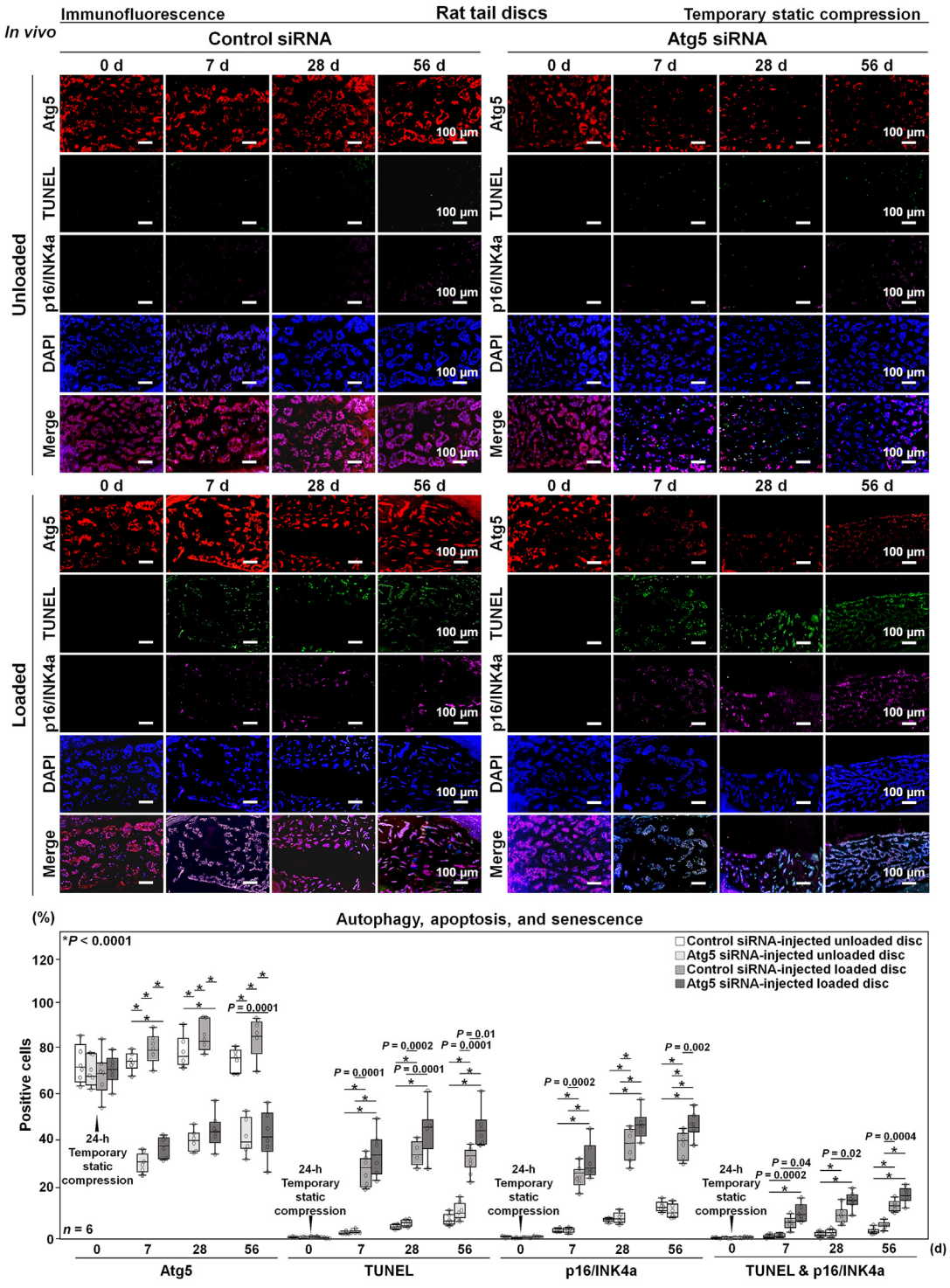

Fig. 6

Osteoarthritis and Cartilage

***In-vivo* Atg5 knockdown enhances immunofluorescent apoptosis and senescence under temporary static compression in rats.** Immunofluorescence for autophagic Atg5 (red), apoptotic TUNEL (green), senescent p16/INK4a (purple), nuclear DAPI (blue), and merged signals of rat tail C11–C12 control siRNA-injected unloaded, C12–C13 Atg5 siRNA-injected unloaded, C8–C9 control siRNA-injected loaded, and C9–C10 Atg5 siRNA-injected loaded discs at 0, 7, 28, and 56 d under temporary static compression at 1.3 MPa for 24 h. Changes in the percentage of Atg5-positive, TUNEL-positive, p16/INK4a-positive, and TUNEL and p16/INK4a-co-positive cells relative to DAPI-positive cells of control siRNA-injected unloaded, Atg5 siRNA-injected unloaded, control siRNA-injected loaded, and Atg5 siRNA-injected loaded discs are shown. Cell count was performed in respective four random LPFs of duplicates. Data are presented with dot and box plots ($n = 6$). Three-way ANOVA with the Tukey–Kramer post-hoc test was used. Immunofluorescent images shown are representative of experiments with similar results.

The observed mechanically induced radiographic, histomorphological, and immunofluorescent disc disruption was further accelerated by Atg5 knockdown in this animal model[29–32]. The lowest disc height, highest degeneration grade, and most prominent apoptosis and senescence induction were observed in Atg5 siRNA-injected loaded discs. Excessive disc NP-cell apoptosis and senescence can lead to disc degeneration through various signaling pathways in response to such stressors as aging, inflammation, nutrient deprivation, and mechanical overloading[46,47]. While progressive disc degeneration was reported by the administration of autophagy inhibitors[25,48], several reports conversely showed promoted disc degeneration possibly by oxidative stress-induced[49] and high lactate concentration-induced[50] autophagy. Thus, roles of autophagy in disc degeneration are still controversial. The present autophagy-inhibition study through Atg5 RNAi, consistently presenting the *in-vitro* and *in-vivo* progression of disc degenerative changes with enhanced apoptosis and senescence, suggests the involvement and importance of Atg5-dependent autophagy in disc cell and tissue homeostasis, consequently the primary role of which is to protect against apoptosis and senescence.

This study has several limitations. The disc disruption mechanism in the used rat tail model is not exactly the same as that in human aging. Rats retain disc-NP notochordal cells throughout their lives unlike adult humans, which could differently respond to mechanical loading[5]. The applied 24-h 1.3-MPa temporary static compression is not physiological, although demonstrating subsequent disc degenerative changes with downregulated *aggrecan* and *Col2a1* gene expression[32]. Then, this study did not evaluate autophagy induction and/or Atg gene overexpression. Further investigation of autophagy activation is warranted to clarify the therapeutic potential for disc degeneration.

In conclusion, the *in-vitro* and *in-vivo* rat intervertebral disc RNAi-mediated loss-of-function study of Atg5 suggests that autophagy maintains homeostasis through cytoprotective effects against apoptosis and senescence. Autophagy could be a new molecular therapeutic target for degenerative disc disease.

Data availability

The data that support the findings of this study are available from the corresponding author upon reasonable request.

Contributions

Conceptualization: Yurube. Data curation: Tsujimoto, Yurube, Takeoka. Formal analysis: Tsujimoto, Yurube, Takeoka, Kanda, K.Miyazaki, Ohnishi, Kakiuchi, S.Miyazaki, Zhang, Takada, Kuroda, Kakutani. Funding acquisition: Yurube, Kuroda, Kakutani. Investigation: Tsujimoto, Yurube, Takeoka, Kanda, K.Miyazaki, Ohnishi, Kakiuchi. Methodology: Tsujimoto, Yurube. Project administration: Yurube. Resources: Yurube, S.Miyazaki, Zhang, Takada, Kakutani. Software: Tsujimoto, Yurube. Supervision: Yurube, Takada, Kuroda, Kakutani. Validation: Tsujimoto, Yurube, Takeoka, Kanda, K.Miyazaki, Ohnishi, Kakiuchi, S.Miyazaki, Zhang, Takada, Kuroda, Kakutani. Writing - original draft: Tsujimoto, Yurube, Takeoka. Writing - review & editing: Kanda, K.Miyazaki, Ohnishi, Kakiuchi, S.Miyazaki, Zhang, Takada, Kuroda, Kakutani.

Conflict of interest

The authors have no competing interests to declare.

Role of the funding source

This work was supported by the Japan Society for the Promotion of Science KAKENHI Grant Numbers JP26893151, JP15H03033, JP15K10406, JP16K20051, and JP21K09323 and a Grant of Japan Orthopaedics and Traumatology Research Foundation, Inc. Number 312. The study sponsors had no involvement in this study.

Acknowledgements

The authors thank Mses. Kyoko Tanaka, Maya Yasuda, and Minako Nagata (Department of Orthopaedic Surgery, Kobe University Graduate School of Medicine, Kobe, Japan) for their technical assistance. We also thank Joseph Iacona, Ph.D. from Edanz Group (https://en-author-services.edanz.com/ac) for editing a draft of this manuscript.

Supplementary data

Supplementary data to this article can be found online at https://doi.org/10.1016/j.joca.2021.12.004.

References

1. Andersson GB. Epidemiological features of chronic low-back pain. Lancet 1999;354:581–5.
2. Martin BI, Deyo RA, Mirza SK, Turner JA, Comstock BA, Hollingworth W, *et al*. Expenditures and health status among adults with back and neck problems. JAMA 2008;299:656–64.
3. Livshits G, Popham M, Malkin I, Sambrook PN, Macgregor AJ, Spector T, *et al*. Lumbar disc degeneration and genetic factors are the main risk factors for low back pain in women: the UK Twin Spine Study. Ann Rheum Dis 2011;70:1740–5.
4. Urban JP, Roberts S. Degeneration of the intervertebral disc. Arthritis Res Ther 2003;5:120–30.
5. Alini M, Eisenstein SM, Ito K, Little C, Kettler AA, Masuda K, *et al*. Are animal models useful for studying human disc disorders/degeneration? Eur Spine J 2008;17:2–19.
6. Choi KS, Cohn MJ, Harfe BD. Identification of nucleus pulposus precursor cells and notochordal remnants in the mouse: implications for disk degeneration and chordoma formation. Dev Dynam 2008;237:3953–8.
7. Boos N, Weissbach S, Rohrbach H, Weiler C, Spratt KF, Nerlich AG. Classification of age-related changes in lumbar intervertebral discs: 2002 Volvo Award in basic science. Spine (Phila Pa 1976) 2002;27:2631–44.
8. Mohanty S, Pinelli R, Pricop P, Albert TJ, Dahia CL. Chondrocyte-like nested cells in the aged intervertebral disc are late-stage nucleus pulposus cells. Aging Cell 2019;18, e13006.
9. Urban JP, Smith S, Fairbank JC. Nutrition of the intervertebral disc. Spine (Phila Pa 1976) 2004;29:2700–9.
10. Antoniou J, Steffen T, Nelson F, Winterbottom N, Hollander AP, Poole RA, *et al*. The human lumbar intervertebral disc: evidence for changes in the biosynthesis and denaturation of the extracellular matrix with growth, maturation, ageing, and degeneration. J Clin Invest 1996;98:996–1003.
11. Danial NN, Korsmeyer SJ. Cell death: critical control points. Cell 2004;116:205–19.
12. Childs BG, Durik M, Baker DJ, van Deursen JM. Cellular senescence in aging and age-related disease: from mechanisms to therapy. Nat Med 2015;21:1424–35.
13. Le Maitre CL, Freemont AJ, Hoyland JA. Accelerated cellular senescence in degenerate intervertebral discs: a possible role in the pathogenesis of intervertebral disc degeneration. Arthritis Res Ther 2007;9. R45.
14. Yurube T, Ito M, Kakiuchi Y, Kuroda R, Kakutani K. Autophagy and mTOR signaling during intervertebral disc aging and degeneration. JOR Spine 2020;3, e1082.
15. Levine B, Kroemer G. Autophagy in the pathogenesis of disease. Cell 2008;132:27–42.

16. Zoncu R, Efeyan A, Sabatini DM. mTOR: from growth signal integration to cancer, diabetes and ageing. Nat Rev Mol Cell Biol 2011;12:21–35.
17. Mizushima N, Yoshimori T, Ohsumi Y. The role of Atg proteins in autophagosome formation. Annu Rev Cell Dev Biol 2011;27:107–32.
18. Mizushima N, Komatsu M. Autophagy: renovation of cells and tissues. Cell 2011;147:728–41.
19. Kabeya Y, Mizushima N, Ueno T, Yamamoto A, Kirisako T, Noda T, *et al.* LC3, a mammalian homologue of yeast Apg8p, is localized in autophagosome membranes after processing. Embo j 2000;19:5720–8.
20. Park I, Chung J, Walsh CT, Yun Y, Strominger JL, Shin J. Phosphotyrosine-independent binding of a 62-kDa protein to the src homology 2 (SH2) domain of p56lck and its regulation by phosphorylation of Ser-59 in the lck unique N-terminal region. Proc Natl Acad Sci U S A 1995;92:12338–42.
21. Klionsky DJ, Abdel-Aziz AK, Abdelfatah S, Abdellatif M, Abdoli A, Abel S, *et al.* (4th edn.)(1). In: Guidelines for the Use and Interpretation of Assays for Monitoring Autophagy, vol. 17. Autophagy; 20211–382.
22. Ito M, Yurube T, Kakutani K, Maeno K, Takada T, Terashima Y, *et al.* Selective interference of mTORC1/RAPTOR protects against human disc cellular apoptosis, senescence, and extracellular matrix catabolism with Akt and autophagy induction. Osteoarthritis Cartilage 2017;25:2134–46.
23. Kakiuchi Y, Yurube T, Kakutani K, Takada T, Ito M, Takeoka Y, *et al.* Pharmacological inhibition of mTORC1 but not mTORC2 protects against human disc cellular apoptosis, senescence, and extracellular matrix catabolism through Akt and autophagy induction. Osteoarthritis Cartilage 2019;27:965–76.
24. Yurube T, Buchser WJ, Moon HJ, Hartman RA, Takayama K, Kawakami Y, *et al.* Serum and nutrient deprivation increase autophagic flux in intervertebral disc annulus fibrosus cells: an in vitro experimental study. Eur Spine J 2019;28:993–1004.
25. Ito M, Yurube T, Kanda Y, Kakiuchi Y, Takeoka Y, Takada T, *et al.* Inhibition of autophagy at different stages by ATG5 knockdown and chloroquine supplementation enhances consistent human disc cellular apoptosis and senescence induction rather than extracellular matrix catabolism. Int J Mol Sci 2021;22:3965.
26. Risbud MV, Shapiro IM. Role of cytokines in intervertebral disc degeneration: pain and disc content. Nat Rev Rheumatol 2014;10:44–56.
27. Nishida K, Doita M, Takada T, Kakutani K, Miyamoto H, Shimomura T, *et al.* Sustained transgene expression in intervertebral disc cells in vivo mediated by microbubble-enhanced ultrasound gene therapy. Spine (Phila Pa 1976) 2006;31:1415–9.
28. Suzuki T, Nishida K, Kakutani K, Maeno K, Yurube T, Takada T, *et al.* Sustained long-term RNA interference in nucleus pulposus cells in vivo mediated by unmodified small interfering RNA. Eur Spine J 2009;18:263–70.
29. Yurube T, Nishida K, Suzuki T, Kaneyama S, Zhang Z, Kakutani K, *et al.* Matrix metalloproteinase (MMP)-3 gene up-regulation in a rat tail compression loading-induced disc degeneration model. J Orthop Res 2010;28:1026–32.
30. Yurube T, Takada T, Suzuki T, Kakutani K, Maeno K, Doita M, *et al.* Rat tail static compression model mimics extracellular matrix metabolic imbalances of matrix metalloproteinases, aggrecanases, and tissue inhibitors of metalloproteinases in intervertebral disc degeneration. Arthritis Res Ther 2012;14.R51.
31. Yurube T, Hirata H, Kakutani K, Maeno K, Takada T, Zhang Z, *et al.* Notochordal cell disappearance and modes of apoptotic cell death in a rat tail static compression-induced disc degeneration model. Arthritis Res Ther 2014;16. R31.
32. Hirata H, Yurube T, Kakutani K, Maeno K, Takada T, Yamamoto J, *et al.* A rat tail temporary static compression model reproduces different stages of intervertebral disc degeneration with decreased notochordal cell phenotype. J Orthop Res 2014;32:455–63.
33. Yurube T, Hirata H, Ito M, Terashima Y, Kakiuchi Y, Kuroda R, *et al.* Involvement of autophagy in rat tail static compression-induced intervertebral disc degeneration and notochordal cell disappearance. Int J Mol Sci 2021;22:5648.
34. Lotz JC, Colliou OK, Chin JR, Duncan NA, Liebenberg E. Compression-induced degeneration of the intervertebral disc: an in vivo mouse model and finite-element study. Spine (Phila Pa 1976) 1998;23:2493–506.
35. Fujita S, Ota E, Sasaki C, Takano K, Miyake M, Miyake J. Highly efficient reverse transfection with siRNA in multiple wells of microtiter plates. J Biosci Bioeng 2007;104:329–33.
36. Risbud MV, Schoepflin ZR, Mwale F, Kandel RA, Grad S, Iatridis JC, *et al.* Defining the phenotype of young healthy nucleus pulposus cells: recommendations of the Spine Research Interest Group at the 2014 annual ORS meeting. J Orthop Res 2015;33:283–93.
37. Gavrieli Y, Sherman Y, Ben-Sasson SA. Identification of programmed cell death in situ via specific labeling of nuclear DNA fragmentation. J Cell Biol 1992;119:493–501.
38. Dimri GP, Lee X, Basile G, Acosta M, Scott G, Roskelley C, *et al.* A biomarker that identifies senescent human cells in culture and in aging skin in vivo. Proc Natl Acad Sci U S A 1995;92:9363–7.
39. Krishnamurthy J, Torrice C, Ramsey MR, Kovalev GI, Al-Regaiey K, Su L, *et al.* Ink4a/Arf expression is a biomarker of aging. J Clin Invest 2004;114:1299–307.
40. Masuda K, Aota Y, Muehleman C, Imai Y, Okuma M, Thonar EJ, *et al.* A novel rabbit model of mild, reproducible disc degeneration by an anulus needle puncture: correlation between the degree of disc injury and radiological and histological appearances of disc degeneration. Spine (Phila Pa 1976) 2005;30:5–14.
41. Lai A, Gansau J, Gullbrand SE, Crowley J, Cunha C, Dudli S, *et al.* Development of a standardized histopathology scoring system for intervertebral disc degeneration in rat models: an initiative of the ORS spine section. JOR Spine 2021;4, e1150.
42. Sasaki H, Takayama K, Matsushita T, Ishida K, Kubo S, Matsumoto T, *et al.* Autophagy modulates osteoarthritis-related gene expression in human chondrocytes. Arthritis Rheum 2012;64:1920–8.
43. Osborn MF, Khvorova A. Improving siRNA delivery in vivo through lipid conjugation. Nucleic Acid Therapeut 2018;28:128–36.
44. Kakutani K, Nishida K, Uno K, Takada T, Shimomura T, Maeno K, *et al.* Prolonged down regulation of specific gene expression in nucleus pulposus cell mediated by RNA interference in vitro. J Orthop Res 2006;24:1271–8.
45. Takeoka Y, Yurube T, Nishida K. Gene therapy approach for intervertebral disc degeneration: an update. Neurospine 2020;17:3–14.
46. Ding F, Shao ZW, Xiong LM. Cell death in intervertebral disc degeneration. Apoptosis 2013;18:777–85.
47. Feng C, Liu H, Yang M, Zhang Y, Huang B, Zhou Y. Disc cell senescence in intervertebral disc degeneration: causes and molecular pathways. Cell Cycle 2016;15:1674–84.
48. Miyazaki S, Kakutani K, Yurube T, Maeno K, Takada T, Zhang Z, *et al.* Recombinant human SIRT1 protects against nutrient deprivation-induced mitochondrial apoptosis through autophagy induction in human intervertebral disc nucleus pulposus cells. Arthritis Res Ther 2015;17:253.

49. Chen JW, Ni BB, Li B, Yang YH, Jiang SD, Jiang LS. The responses of autophagy and apoptosis to oxidative stress in nucleus pulposus cells: implications for disc degeneration. Cell Physiol Biochem 2014;34:1175–89.

50. Wu W, Zhang X, Hu X, Wang X, Sun L, Zheng X, *et al*. Lactate down-regulates matrix systhesis and promotes apoptosis and autophagy in rat nucleus pulposus cells. J Orthop Res 2014;32:253–61.